Glucose-dependent signalling pathways regulate TE differentiation in bovine embryos

Jinlong Qiu[1] and Roger Sturmey[1#]

1. Centre for Biomedicine, Hull York Medical School, University of Hull, Hull, HU6 7RX, UK

Authors for correspondence (Roger.Sturmey@hyms.ac.uk)

Abstract

Glucose uptake and metabolism increase markedly during the transition from morula to blastocyst. However, the functional roles of glucose during this process in bovine embryos remain incompletely understood. Here, we demonstrate that glucose specifically modulates trophectoderm (TE) differentiation without affecting the inner cell mass (ICM), acting through Hippo signalling via the hexosamine biosynthetic pathway (HBP) and the pentose phosphate pathway (PPP) rather than glycolysis. Consistently, scRNA-seq analysis reveals that glycolysis-related genes show only stage-specific changes, whereas HBP- and PPP-related genes exhibit both stage- and lineage-specific differences between TE and ICM. Furthermore, we found that glucose deprivation does not impair pyruvate uptake or intracellular pyruvate levels in blastocysts, yet it significantly depletes the terminal metabolites of the HBP. Together, these findings reveal that glucose-dependent regulation of TE differentiation is conserved in bovine embryos.

Introduction

Glucose is a key metabolic substrate during early embryonic development [1, 2]. Classical models of glucose metabolism presumed that glucose is predominantly catabolized through glycolysis to generate pyruvate, which enters the tricarboxylic acid (TCA) cycle to satisfy the energetic requirements of cell proliferation and development [3, 4].

However, recent studies in mouse embryos have challenged this traditional bioenergetic view of glucose metabolism [5-7]. These studies demonstrate that, during early preimplantation development, glucose contributes only minimally to glycolytic flux and ATP production [5-7]. Instead, glucose-derived carbon is preferentially channeled into HBP and PPP, supporting biosynthetic processes and redox homeostasis [5, 7].

In particular, HBP-derived O-linked N-acetylglucosaminylation (O-GlcNAc) has been implicated in the regulation of the Hippo signaling pathway, thereby influencing TE-associated transcriptional programs [5, 8, 9]. In parallel, the PPP has been shown to function upstream of mechanistic target of rapamycin (mTOR) signaling to regulate TE specification [5, 10, 11]. Notably, whether this glucose-driven signaling paradigm is conserved in bovine embryos, remains unclear.

In this study, we demonstrate that although glucose-mediated regulation of the TE program is conserved in bovine embryos, their metabolic dependency appears substantially more complex than that observed in murine models. Notably, bovine embryos exhibit a greater tolerance to glucose deprivation, as blastocyst formation can still occur in the absence of glucose. Furthermore, the contributions of HBP and PPP appear to be highly context-dependent, with developmental outcomes varying according to the specific stage at which inhibition occurs and the metabolic nodes targeted. Collectively, our findings highlight a critical role for glucose in TE formation in large mammals while revealing a sophisticated and complex metabolic regulatory network underlying this process.

55 ## Materials and methods

56 Unless specified otherwise, all reagents and chemicals were obtained from Merck
57 (Dorset, UK).

58 ### In vitro bovine embryo production

59 In vitro maturation (IVM), fertilization (IVF), and culture (IVC) of bovine embryos were
60 performed according to previously described protocols with minor modifications [12-
61 14]. IVM, IVF, and SemenPrep media were obtained from IVF Bioscience (Falmouth, UK).
62 Bovine ovaries were harvested from animals slaughtered for commercial purposes
63 unrelated to the study. Ovaries were collected and transported to the laboratory within 2
64 hours of slaughter. Cumulus–oocyte complexes (COCs) were collected from 3–8 mm
65 follicles on the ovarian surface. COCs were cultured in IVM medium at 38.5°C, 5% CO_2
66 for 22 hours. Following maturation, groups of 25–30 COCs were co-incubated with
67 spermatozoa (Genus Plc) (1–5 × 10^6/mL) purified from frozen–thawed semen using
68 SemenPrep medium. IVF was carried out at 38.5°C, 5% CO_2 for 10–14 hours. After
69 fertilization, cumulus cells were removed. Presumptive zygotes were subsequently
70 cultured in BO-SOF medium supplemented with either 0 mM or 1.5 mM glucose at
71 39 °C, 5% CO_2 and 5% O_2.

72 The BO-SOF formulation was prepared according to the protocol described in our
73 previous publication [15, 16]. The concentrations were selected based on previously
74 published studies [5, 17]. The inhibitors used in this study are listed in Supplementary
75 Table 1. Unless otherwise stated, inhibitors were added from E0.

76 ### Metabolic assay

77 Morula-stage embryos were individually cultured for 24 hours in 5-µL microdrops, after
78 which embryos that successfully developed to the blastocyst stage were identified and
79 their spent culture media were collected. All samples were immediately stored at −78°C
80 until subsequent metabolic assays. Pyruvate concentrations were quantified using
81 enzyme-coupled fluorometric methods adapted from a previously established protocol
82 [15]. All enzymes used for metabolic analyses were obtained from Roche (Burgess Hill,
83 UK). Standard curves were generated from serial dilutions of freshly prepared

metabolite standards. Fluorescence values were calculated as the difference between pre- and post-incubation readings and converted to absolute concentrations. All measurements were performed in technical triplicate, and assays with standard curve R^2 values < 0.98 were excluded from further analysis.

Measurement of Basal Oxygen Consumption Rate (OCR)

The OCR detection protocol is based on previously published articles [16]. Briefly, OCR was assessed using a Seahorse XFp Analyzer (Agilent Technologies). Seahorse analysis was performed following the manufacturer's recommendations for OCR. Embryos were allocated in small groups (6-10 bovine blastocysts per well) in 180 µl of HEPES-buffered SOF medium appropriate for the developmental stage.

JC-1 staining

JC-1 (Thermo Fisher) was initially dissolved in DMSO and subsequently diluted to a final concentration of 1 µM in SOF medium. Embryos were incubated in this solution for 30 minutes under standard culture conditions. Following three washes with HEPES-buffered SOF, the embryos were imaged using a Zeiss LSM710 confocal microscope.

IF

Samples were first washed three times with 0.1% polyvinylpyrrolidone/phosphate-buffered saline (PBS), then fixed with 4% paraformaldehyde/PBS for 30 minutes and then permeabilized with 0.5% Triton X-100/PBS for 30 minutes at room temperature. The blocking step was performed in blocking buffer (PBS containing 10% FBS and 0.1% Triton X-100) for 1 hour. Afterwards, samples were incubated overnight with primary antibodies in blocking buffer at 4°C. After three washes, embryos were incubated with secondary antibodies for 2 hours. Finally, samples were stained with Hoechst3342 (Hoechst) (Merck) for 30 minutes and then mounted. Images were acquired using inverted fluorescence microscope (Zeiss AXIO Vert.A1) or a laser scanning confocal microscope (Zeiss LSM 710) with a 40x objective lens.

FIJI (https://imagej.net/software/fiji/) was used for image visualization, cell counting, and signal intensity measurements. Depending on the experiment, signal intensity was

measured and background subtracted to analyze absolute intensity. All antibodies (Supplementary Table S2 and S3) were validated to react with bovine cells [12, 18, 19].

Single-cell RNA-seq data acquisition and processing

The single-cell RNA sequencing (scRNA-seq) dataset of bovine preimplantation embryos analyzed in this study was obtained from the publicly available Gene Expression Omnibus (GEO) database under accession number GSE239782 [20]. This dataset contains transcriptomic profiles of bovine embryos at defined developmental stages, including morula, early blastocyst, mid-blastocyst, and late blastocyst stages. Raw count matrices were downloaded and processed using the Seurat R package (version 4.5.2). The calculation of module scores and all analysis codes were adapted from previously published studies [21].

Statistical Analysis

Unless otherwise noted, all experiments were performed with at least three biological replicates. Differences between groups were evaluated using two-tailed unpaired Student's t-tests. Graphs were generated with GraphPad Prism 10.

Results

Glucose is essential for blastocyst formation

Embryos were cultured from embryonic day 0 (E0) in glucose-free medium (G−) or in medium supplemented with 1.5 mM glucose (CTRL). No significant differences were observed in developmental rates at the 4-cell stage (E2.0), the 8–16-cell stage (E3.5), or the morula stage (E5.0) between G− and CTRL embryos (Fig. 1A, B). However, blastocyst formation in the G− group was markedly reduced at E6.5 (Fig. 1A, B), and the total cell numbers of blastocysts were significantly decreased, with this decline already apparent at the morula stage (Fig. S1A–D). Notably, the few G− embryos that reached the blastocyst stage failed to hatch normally at E8.5 (Fig. 1C, D). Inhibition of glucose metabolism using the hexokinase inhibitor 2-deoxy-D-glucose (2-DG) similarly reduced

139 blastocyst rate, confirming the important role of glucose in blastocyst formation (Fig.
140 S1F, G).

141 To dissect the contributions of different glucose metabolic pathways, specific inhibitors
142 were used to block glycolysis, HBP, and PPP (Fig. S1E). Inhibiting glucose flux into
143 pyruvate with YZ9 had no effect on blastocyst formation (Fig. 1E, F). In contrast,
144 blocking the PPP with 6-aminonicotinamide (6-AN) or the HBP with 6-Diazo-5-oxo-L-
145 norleucine (DON) induced morula-stage developmental arrest, which could not be
146 rescued by supplementation with their downstream metabolites (Fig. S1H–K). However,
147 inhibition of the downstream HBP enzyme O-GlcNAc transferase (OGT) using
148 ST045849(TT04) had no effect on blastocyst formation (Fig. 1G, H). In addition, when
149 PPP inhibition was delayed until E5.5, embryos were able to reach the blastocyst stage,
150 although the blastocyst formation rate was significantly reduced (Fig. 1I, J). Together,
151 these results demonstrate that glucose plays a role in blastocyst formation, with
152 distinct contributions from its metabolic branches.

153 **Glucose metabolism regulates TE through Hippo pathway**

154 Immunofluorescence analysis was performed on E7.0 blastocysts cultured under CTRL
155 or G− conditions to assess the abundance of key lineage-specific transcription factors
156 (Fig 2A). Quantitative analysis revealed that glucose deprivation significantly reduced the
157 fluorescence intensity of the TE marker CDX2 (Fig 2B) and decreased the proportion of
158 $CDX2^+$ cells within the blastocyst (Fig 2C). Consistently, expression of an additional TE
159 marker, GATA3, was also reduced under G- conditions (Fig S 2A, B).

160 In contrast, neither the expression level of the ICM marker SOX2 nor the proportion of
161 $SOX2^+$ cells was significantly altered (Fig. 2B, C). Consistently, the expression levels and
162 cell numbers of the epiblast (EPI) marker NANOG and the primitive endoderm (PrE)
163 marker GATA6 were comparable between groups (Fig. 2D–F), indicating that glucose
164 predominantly affects TE differentiation rather than ICM lineage specification.

165 Given the central role of Hippo signalling in TE specification [22, 23], Hippo pathway
166 activity was next examined. Immunofluorescence analyses revealed a significant
167 reduction in phosphorylated YAP (p-YAP) levels in G- embryos (Fig 2I, J). Consistently,
168 nuclear localisation of YAP, as well as the TE-associated transcription factors TFAP2C and

169 TEAD4, was decreased under G- conditions (Fig 2G, H, K, L), indicating that glucose
170 regulates TE through Hippo pathway.

171 Similar phenotypes were observed following inhibition of glucose metabolism 2-DG.
172 Treatment with 2-DG significantly reduced total cell numbers and altered the TE-to-ICM
173 cell ratio in E7.0 blastocysts (Fig S 2E), accompanied by selective suppression of CDX2
174 expression without affecting SOX2 levels (Fig S 2C–F). Moreover, expression of YAP,
175 TFAP2C, and p-YAP was significantly decreased following 2-DG treatment (Fig S 2G–J),
176 supporting the conclusion that glucose specifically regulates TE differentiation via Hippo
177 signalling.

178

179 **Glucose availability regulates HBP activity and epigenetic landscapes**

180 To investigate the metabolic mechanisms by which glucose regulates TE differentiation
181 via the Hippo pathway, we re-analyzed publicly available metabolomics datasets from
182 bovine blastocysts cultured under CTRL and G− conditions [24]. Glucose deprivation
183 led to a broad reduction in intermediate metabolites across glycolysis, HBP and PPP
184 (Fig. S3A). However, the end products of glycolysis and PPP remained unchanged, as
185 pyruvate and ribose levels were unaffected (Fig. S3A). In contrast, HBP metabolites,
186 including N-acetylglucosamine (GlcNAc) and UDP-GlcNAc, were markedly reduced
187 (Fig. S3A), highlighting a selective vulnerability of the HBP to glucose deprivation.

188 To validate our metabolomics findings, we first measured mitochondrial membrane
189 potential (ΔΨm) to assess the impact of glucose availability on cellular energy
190 homeostasis. Glucose deprivation significantly reduced the orange/green JC-1
191 fluorescence ratio in bovine blastocysts, indicative of mitochondrial depolarization (Fig
192 3A, B). However, basal oxygen consumption rates (OCR) measured by Seahorse
193 analysis were comparable between G– and CTRL embryos (Fig 3C). This suggests that
194 while glucose is essential for maintaining mitochondrial membrane potential, the
195 embryos may sustain basal respiratory flux through the utilization of alternative
196 metabolic substrates [25, 26].

To determine whether embryos compensate for the absence of glucose by increasing reliance on exogenous pyruvate, pyruvate consumption from the culture medium was assessed. Measurement of pyruvate concentrations in spent culture media revealed no significant differences between CTRL and G- embryos (Fig 3D). Consistently, 2-DG or YZ9 inhibition did not significantly alter pyruvate concentration as well (Fig 3E, F). Collectively, these findings indicate that embryos do not trigger a compensatory increase in exogenous pyruvate uptake to offset the energy deficit caused by glucose deprivation.

To validate the impact of glucose deprivation on the HBP identified in our metabolomics re-analysis, we assessed global O-GlcNAc levels via immunofluorescence. Consistent with the marked depletion of HBP metabolites, O-GlcNAc levels were significantly reduced in blastocysts cultured under G- conditions or treated with 2-DG (Fig 3G, H and Fig S 3C, D). These results confirm that restricted glucose availability directly compromises HBP-mediated protein glycosylation in bovine embryos.

In parallel, metabolomics re-analysis revealed significant alterations in metabolites associated with amino acid methylation, including those linked to lysine trimethylation (Kme3) and arginine methylation (ADMA and SDMA) (Fig. S3B). Guided by these observations, we examined the impact of glucose deprivation and metabolic inhibition on epigenetic modifications. Both glucose deprivation and 2-DG treatment markedly reduced ADMA and SDMA levels, accompanied by a pronounced decrease in the repressive histone mark H3K27me3 (Fig. 3I–N and Fig. S3C–J). These findings indicate that glucose availability is a key determinant of the epigenetic landscape in bovine blastocysts.

HBP-Dependent O-GlcNAc Regulates CDX2

To determine whether the HBP signaling axis operates through O-GlcNAc during bovine blastocyst development, we first confirmed that TT04 treatment significantly reduced global O-GlcNAc levels (Fig. 4G, H). We then assessed the impact of O-GlcNAc inhibition on lineage specification. TT04 treatment specifically decreased CDX2

226 expression without affecting SOX2 levels (Fig. 4A, B), while total cell number and the
227 relative proportions of TE and ICM cells remained unchanged (Fig. 4C, D).

228 Given the reduction in CDX2 expression, we next examined the Hippo signaling
229 pathway. TT04 treatment significantly reduced total YAP protein levels without altering
230 TFAP2C expression (Fig. 4E, F). In addition, TT04 markedly increased phosphorylated
231 YAP (p-YAP) levels (Fig. 4G, H), indicating enhanced YAP phosphorylation and
232 cytoplasmic retention upon O-GlcNAc inhibition.

233 Collectively, these findings demonstrate that O-GlcNAc acts as a key metabolic signal
234 that maintains TE identity by stabilizing YAP and preventing its phosphorylation.

235

236 **A PPP–mTOR Pathway Regulates TFAP2C**

237 Glucose-derived nucleotides generated via the PPP act as nutrient signals that activate
238 mTOR signaling [5, 27]. To assess mTORC1 activity under glucose deprivation or PPP
239 inhibition, phosphorylated ribosomal protein S6 (pS236-RPS6) was used as a
240 downstream readout. Immunofluorescence analysis revealed a marked reduction in
241 pS236-RPS6 levels in both G− and 6-AN–treated blastocysts compared with CTRL
242 embryos (Fig. 5A–D), indicating that PPP activity is required to sustain mTORC1
243 signaling during bovine blastocyst development.

244 Given that mTOR promotes mRNA translation through phosphorylation of 4E-BP1 and
245 RPS6 [5, 10, 11], we next examined whether PPP regulates TFAP2C expression via
246 mTOR. Embryos were treated with the mTOR inhibitor INK128 from E5.5, which
247 effectively suppressed mTORC1 activity, as evidenced by reduced pS236-RPS6 levels
248 (Fig. 5G, H). Notably, mTOR inhibition did not affect the overall blastocyst formation rate
249 (Fig. 5E, F), but significantly reduced TFAP2C and CDX2 expression (Fig. 5I, J).
250 Quantitative analysis further revealed a reduction in total blastocyst cell number
251 following INK128 treatment, primarily due to a loss of TE ($CDX2^{+}$) cells, while ICM
252 ($CDX2^{-}$) cell numbers remained unchanged (Fig. 5K). Collectively, these findings
253 identify mTORC1 as a key glucose-responsive signaling node that links PPP-derived
254 nucleotide metabolism to TFAP2C expression and TE lineage expansion.

255

256 **Single-cell transcriptomic profiling reveals lineage-specific metabolic signatures**
257 **in bovine blastocysts**

258 To further delineate the metabolic dynamics during bovine preimplantation
259 development and corroborate our in vitro findings, we analyzed single-cell
260 transcriptomic data spanning from the morula to the late blastocyst stages. UMAP
261 dimensionality reduction successfully reconstructed the developmental trajectory and
262 clearly segregated the distinct early embryonic cell lineages, including the TE, ICM, EPI,
263 and PE (Fig. S4A). Heatmap analysis of metabolic gene modules revealed that oxidative
264 phosphorylation (OXPHOS), glycolysis, the HBP, and the PPP exhibit distinct stage- and
265 lineage-specific expression patterns during early embryogenesis (Fig. S4C and Fig 6 A,
266 D, G). To robustly quantify these pathway-level changes and overcome the sparsity of
267 single-cell data, we calculated metabolic module scores, which reflect the overall
268 transcriptional enrichment of these entire metabolic networks within individual cells.

269 To establish a macroscopic understanding of the metabolic landscape, we first
270 evaluated the comprehensive module scores across all identified developmental
271 stages and cell lineages (Fig. S4B). This overview revealed that OXPHOS maintains a
272 consistently high and relatively stable transcriptional baseline throughout
273 preimplantation development, likely fulfilling the basal energetic demands of the
274 embryo. In contrast, the glucose-driven pathways displayed lower overall absolute
275 scores but exhibited highly dynamic fluctuations, prompting us to further dissect their
276 stage- and lineage-specific variations (Fig. S4B).

277 We next quantitatively assessed the dynamic shifts in these metabolic modules as
278 embryos progressed through preimplantation development. Bar graphs comparing
279 grouped stages revealed that during the transition from the morula to the mid-
280 blastocyst (MB) stage, the expression modules for both OXPHOS and glycolysis
281 generally increased (Fig. S4D and Fig 6B). However, at the late blastocyst (LB) stage,
282 OXPHOS scores underwent a significant decline, whereas glycolysis continued to
283 sharply rise (Fig. S4D and Fig 6B). This divergent pattern indicates a fundamental
284 metabolic switch in energy production strategies, transitioning toward a predominantly

285 glycolytic state, which is highly consistent with previously reported metabolic shifts in
286 mammalian embryogenesis [21, 28-30].

287 In contrast to the continuous trajectory of glycolysis, the dynamic changes of the
288 glucose-driven anabolic branches, HBP and PPP, were more complex. The HBP score
289 initially exhibited a transient dip at the early blastocyst (EB) stage before steadily
290 upregulating and peaking at the LB stage (Fig. 6F). Similarly, the PPP module showed a
291 high baseline at the morula stage, followed by a decline at the EB stage, and a
292 subsequent recovery and continuous increase through the MB and LB stages (Fig. 6H).
293 Collectively, these results indicate that glucose-driven metabolic pathways undergo
294 pronounced fluctuations during the morula-to-blastocyst transition.

295 Importantly, we investigated whether these glucose-driven pathways exhibited lineage-
296 specific partitioning corresponding to our in vitro phenotypes. Quantitative comparison
297 of module scores revealed highly nuanced, pathway-specific metabolic wiring among
298 the cell lineages at the mid- and late-blastocyst stages (Fig. S4B). Notably, the
299 glycolysis scores showed no significant differences between the TE and ICM lineages
300 (Fig. 6C). This finding perfectly aligns with our earlier in vitro observation that inhibiting
301 high-flux glycolysis with YZ9 does not selectively impair TE specification (Fig. S2K, M),
302 confirming that basal glycolysis is broadly utilized rather than acting as a lineage-
303 determining driver.

304 In stark contrast, the HBP module was robustly and specifically enriched in the TE
305 compared to the ICM at the critical mid-blastocyst stage (Fig. 6F). This striking
306 differential expression provides compelling in vivo transcriptomic evidence that HBP
307 activity is preferentially partitioned to the TE, mechanistically explaining why TE
308 specification relies heavily on the HBP-O-GlcNAc-YAP signaling axis.

309 In addition, the PPP module displayed high activity in both embryonic lineages. Notably,
310 the module score in the MB ICM was significantly higher than that in MB TE, whereas LB
311 TE scores were significantly higher than LB PE (Fig. 6I). This dynamic lineage-specific
312 shift suggests that both ICM and TE rely on PPP during blastocyst development, albeit
313 with different temporal requirements. The elevated PPP activity likely reflects the
314 increased demand for nucleotide biosynthesis and redox homeostasis required to

sustain rapid cellular proliferation [4, 5, 31, 32]. Consequently, inhibition of PPP is expected to affect both lineages and may therefore produce more severe developmental phenotypes than inhibition of other glucose-derived pathways. This robust and ubiquitous expression pattern perfectly aligns with our in vitro observations: pharmacological suppression of the PPP using 6-AN starting from the zygote stage results in a catastrophic developmental arrest at the morula stage (Fig S1H, I).

Discussion

In this study, we demonstrate that bovine embryos exhibit a markedly higher tolerance to glucose deprivation compared with murine models. Although the absence of glucose significantly reduced blastocyst formation rates and compromised overall embryo quality, a subset of embryos retained the capacity to progress beyond the morula stage and form blastocysts (Fig. 1A, B). This contrasts sharply with mouse embryos, which undergo irreversible developmental arrest at the morula stage upon glucose deprivation [2, 5]. In mice, this developmental arrest is generally attributed to impaired glucose-dependent regulation of CDX2 expression through the Hippo signaling pathway, which consequently prevents blastocoel formation [2, 5]. However, in bovine embryos, while the Hippo pathway–dependent regulation of CDX2 is conserved [23], CDX2 disruption does not preclude blastocyst formation [14, 33]. Accordingly, although glucose deficiency markedly suppresses the expression of key TE transcription factors, including CDX2 and GATA3, bovine embryos can still form blastocysts even under glucose-deprived conditions (Fig. 2A, 2B and Fig S2A, S2B).

In addition, our findings demonstrate that the three main pathways of glucose metabolism fulfill unique functional roles during TE differentiation. We found that basal OCR and exogenous pyruvate uptake remained stable in G− embryos (Fig. 3C–F), and inhibition of glucose flux into pyruvate using YZ9 did not impair blastocyst formation and TE specification (Fig. 1E, F). This phenotype may be explained by the distinct metabolic resilience of bovine embryos. Unlike murine embryos, which contain relatively low lipid reserves, bovine embryos possess abundant lipid droplets that can serve as alternative energy and biosynthetic substrates under glucose-deprived

conditions [25, 34, 35]. Moreover, the BO-SOF culture medium used in this study provides sufficient levels of pyruvate, lactate, and amino acids, which likely compensate for glucose deprivation by providing alternative metabolic fuels [36-38].

Nevertheless, endogenous lipid reserves and exogenous nutrients in the culture medium are insufficient to fully offset the absence of glucose. We observed that glucose deprivation, or the pharmacological inhibition of its metabolism, significantly attenuated HBP-mediated O-GlcNAc (Figure 3G, H and S3 A, C, D). In murine embryos, O-GlcNAc has been proposed to primarily facilitate the nuclear stabilization of YAP, independent of its intracytoplasmic phosphorylation status [5, 8, 39]. When YAP is phosphorylated, it remains localized in the cytoplasm where it undergoes degradation. This exclusion from the nucleus inhibits the expression of TE-associated genes [22, 23]. However, in contrast to this model, we observed that inhibition of O-GlcNAc using TT04 significantly increased p-YAP levels (Fig. 4G, 4H). Concurrently, the inhibition also significantly reduced nuclear YAP accumulation and downregulated CDX2 expression (Figure 4 A-F). The relationship between glycosylation and YAP phosphorylation during embryogenesis is largely unexplored. However, mutating the Thr241 O-GlcNAc site significantly compromises YAP stability while promoting its phosphorylation in tumor cells [40]. We therefore speculate that inhibition of O-GlcNAc promotes YAP retention in the cytoplasm in bovine embryos, where it becomes increasingly phosphorylated. Interestingly, unlike HBP-specific inhibition, glucose deprivation in bovine embryos resulted in a marked reduction in p-YAP (Fig. 1I, 1J). In cancer cells, AMPK-mediated site-specific phosphorylation serves as a primary mediator of glucose-deficiency signaling [41, 42]. Thus, we speculate that glucose deprivation reduces overall phosphorylation levels, leading to decreased p-YAP.

The role of glucose in regulating phosphorylation is further supported by its impact on the mTOR pathway [42]. We found that glucose deprivation significantly decreased phosphorylation of RPS6, a downstream target of mTORC1 (Figure 5A, B). In addition, inhibition of PPP disrupted mTOR signaling, and both PPP inhibition and mTOR suppression markedly reduced the expression of the TE-associated transcription factor TFAP2C (Fig. 5G-K). These findings indicate that PPP activity is essential for maintaining the mTORC1–TFAP2C signaling axis required for proper TE differentiation.

Furthermore, inhibition of PPP from the zygote stage resulted in developmental arrest at the morula stage, which could not be rescued by supplementation with downstream metabolites (Fig. S1H–K). Glucose flux through the PPP serves a critical antioxidant function via NADPH production [31, 32]. When this pathway is disrupted at the G6PD level, murine embryos experience elevated ROS levels [5, 31]. While uridine can mitigate some defects, full phenotypic restoration requires a combinatorial approach addressing both nucleotide depletion and oxidative stress [5]. We thus speculate that the irreversible arrest observed in bovine embryos is due to elevated reactive oxygen species (ROS) levels induced by pathway inhibition, ultimately leading to embryonic lethality.

Beyond direct signaling cascades, glucose availability profoundly shapes the embryonic epigenetic landscape. We observed that disrupted glucose metabolism led to significant reductions in arginine methylation (ADMA and SDMA) alongside a pronounced decrease in the repressive histone modification H3K27me3 (Fig. 3I–N and Fig. S3E–H). Protein arginine methyltransferase 1 (PRMT1) accounts for approximately 85% of ADMA formation in cells [43, 44]. By inhibiting phosphorylation-dependent cytoplasmic retention and proteasomal degradation, PRMT1-mediated methylation promotes YAP stabilization and nuclear accumulation [45]. Therefore, we speculate that glucose may interfere with the Hippo pathway by affecting arginine methylation, thereby influencing TE differentiation. Collectively, our findings highlight a potential link between glucose metabolism and epigenetic control, providing a new avenue for investigating the mechanisms underlying lineage specification.

Publicly available data support our model: glucose deprivation selectively impacts glycosylation-related metabolites without reducing pyruvate levels (Figure S3 A, B). Furthermore, single-cell analysis shows that the HBP and PPP, but not glycolysis, are differentially regulated between the TE and ICM (Figure 6 A-H). In conclusion, our results demonstrate that glucose specifically regulates TE differentiation in bovine embryos, primarily through its flux into the HBP and PPP.

Acknowledgements

We thank Prof. Henry J Leese for his helpful discussion.

Competing interests

The authors declare no competing or financial interests.

Author contributions

J.Q. conceived the project, designed and performed all experiments, analysed and interpreted the data, and drafted and critically revised the manuscript. R.S. secured funding for the project and critically revised the manuscript.

Funding

There were no project specific funds for this work. Reagents used in this study were provided by the R.S. laboratory through general laboratory funds.

References

1. M.L. Sutton-McDowall, J.G.T., *Metabolism in the pre-implantation oocyte and embryo*. Animal Reproduction, 2015.
2. Brown, J.J. and D.G. Whittingham, *The roles of pyruvate, lactate and glucose during preimplantation development of embryos from F1 hybrid mice in vitro*. Development, 1991. **112**(1): p. 99-105.
3. Werner, C., T. Doenst, and M. Schwarzer, *Chapter 4 - Metabolic Pathways and Cycles*, in *The Scientist's Guide to Cardiac Metabolism*, M. Schwarzer and T. Doenst, Editors. 2016, Academic Press: Boston. p. 39-55.
4. Stincone, A., et al., *The return of metabolism: biochemistry and physiology of the pentose phosphate pathway*. Biol Rev Camb Philos Soc, 2015. **90**(3): p. 927-63.
5. Chi, F., et al., *Glycolysis-Independent Glucose Metabolism Distinguishes TE from ICM Fate during Mammalian Embryogenesis*. Dev Cell, 2020. **53**(1): p. 9-26 e4.
6. Biggers, J.D., D.G. Whittingham, and R.P. Donahue, *The pattern of energy metabolism in the mouse oöcyte and zygote*. Proceedings of the National Academy of Sciences, 1967. **58**(2): p. 560-567.
7. O'Fallon, J.V. and R.W. Wright, Jr., *Quantitative determination of the pentose phosphate pathway in preimplantation mouse embryos*. Biol Reprod, 1986. **34**(1): p. 58-64.
8. Peng, C., et al., *Regulation of the Hippo-YAP Pathway by Glucose Sensor O-GlcNAcylation*. Molecular Cell, 2017. **68**(3): p. 591-604.e5.
9. Scrivener, A.L., et al., *Protein O-GlcNAcylation in reproductive biology and the impact of metabolic disease*. Human Reproduction Update, 2025. **31**(5): p. 512-531.
10. Düvel, K., et al., *Activation of a Metabolic Gene Regulatory Network Downstream of mTOR Complex 1*. Molecular Cell, 2010. **39**(2): p. 171-183.
11. Simcox, J. and D.W. Lamming, *The central moTOR of metabolism*. Developmental Cell, 2022. **57**(6): p. 691-706.
12. Li, S., et al., *Linker histone H1FOO is required for bovine preimplantation development by regulating lineage specification and chromatin structuredagger*. Biol Reprod, 2022. **107**(6): p. 1425-1438.
13. Dang, Y., et al., *The lysine deacetylase activity of histone deacetylases 1 and 2 is required to safeguard zygotic genome activation in mice and cattle*. Development, 2022. **149**(11).
14. Shi, Y., et al., *Functional role of GATA3 and CDX2 in lineage specification during bovine early embryonic development*. Reproduction, 2023.
15. Guerif, F., et al., *A simple approach for COnsumption and RElease (CORE) analysis of metabolic activity in single mammalian embryos*. PLoS One, 2013. **8**(8): p. e67834.
16. Muller, B., et al., *Application of extracellular flux analysis for determining mitochondrial function in mammalian oocytes and early embryos*. Scientific Reports, 2019. **9**(1): p. 16778.
17. Cao, D., et al., *Selective utilization of glucose metabolism guides mammalian gastrulation*. Nature, 2024. **634**(8035): p. 919-928.

18. Wu, X., et al., *TEAD4 regulates KRT8 and YAP in preimplantation embryos in mice but not in cattle*. Reproduction, 2024. **167**(3).
19. Li, S., et al., *NOTCH signaling pathway is required for bovine early embryonic developmentdagger*. Biol Reprod, 2021. **105**(2): p. 332-344.
20. Hu, B., et al., *Single-cell RNA-Seq reveals the earliest lineage specification and X chromosome dosage compensation in bovine preimplantation embryos*. FASEB J, 2024. **38**(4): p. e23492.
21. Malkowska, A., et al., *A hexa-species transcriptome atlas of mammalian embryogenesis delineates metabolic regulation across three different implantation modes*. Nature Communications, 2022. **13**(1).
22. Wu, Z. and K.-L. Guan, *Hippo Signaling in Embryogenesis and Development*. Trends in Biochemical Sciences, 2021. **46**(1): p. 51-63.
23. Gerri, C., et al., *A conserved role of the Hippo signalling pathway in initiation of the first lineage specification event across mammals*. Development, 2023. **150**(8).
24. Uhde, K., et al., *Exposure to elevated glucose concentrations alters the metabolomic profile of bovine blastocysts*. PLOS ONE, 2018. **13**(6): p. e0199310.
25. Herrick, J.R., et al., *Developmental and molecular response of bovine embryos to reduced nutrients in vitro*. Reproduction and Fertility, 2020. **1**(1): p. 51-65.
26. Krisher, R.L. and J.R. Herrick, *Bovine embryo production in vitro: evolution of culture media and commercial perspectives*. Anim Reprod, 2024. **21**(3): p. e20240051.
27. Ma, C., et al., *mTOR hypoactivity leads to trophectoderm cell failure by enhancing lysosomal activation and disrupting the cytoskeleton in preimplantation embryo*. Cell Biosci, 2023. **13**(1): p. 219.
28. Thompson, J.G., et al., *Oxygen uptake and carbohydrate metabolism by in vitro derived bovine embryos*. J Reprod Fertil, 1996. **106**(2): p. 299-306.
29. Banliat, C., et al., *The proteomic analysis of bovine embryos developed in vivo or in vitro reveals the contribution of the maternal environment to early embryo*. BMC Genomics, 2022. **23**(1): p. 839.
30. Traut, M., et al., *Deregulation of oxidative phosphorylation pathways in embryos derived in vitro from prepubertal and pubertal heifers based on whole-transcriptome sequencing*. BMC Genomics, 2024. **25**(1): p. 632.
31. Warzych, E., P. Lipinska, and E. Sell-Kubiak, *Pentose phosphate pathway inhibition during in vitro maturation substantially affects the metabolism of bovine COCs and blastocysts*. Theriogenology, 2024. **230**: p. 72-80.
32. Braga, J.V., et al., *The role of the pentose phosphate pathway on reproductive functions*. Anim Reprod, 2025. **22**(4): p. e20240130.
33. Goissis, M.D. and J.B. Cibelli, *Functional characterization of CDX2 during bovine preimplantation development in vitro*. Molecular Reproduction and Development, 2014. **81**(10): p. 962-970.
34. Barceló-Fimbres, M. and G.E. Seidel, *Cross-validation of techniques for measuring lipid content of bovine oocytes and blastocysts*. Theriogenology, 2011. **75**(3): p. 434-444.
35. Kajdasz, A., et al., *Lipid Stores and Lipid Metabolism Associated Gene Expression in Porcine and Bovine Parthenogenetic Embryos Revealed by Fluorescent Staining and RNA-seq*. Int J Mol Sci, 2020. **21**(18).

36. Pasquariello, R., et al., *Lipid Enriched Reduced Nutrient Culture Medium Improves Bovine Blastocyst Formation*. Reprod Fertil, 2023. **4**(4).
37. Sudano, M.J., et al., *Lipid content and apoptosis of in vitro-produced bovine embryos as determinants of susceptibility to vitrification*. Theriogenology, 2011. **75**(7): p. 1211-1220.
38. Ordoñez-Leon, E.A., et al., *Lipid droplet analysis using in vitro bovine oocytes and embryos*. Reprod Domest Anim, 2014. **49**(2): p. 306-14.
39. Lei, Y., et al., *Protein O-GlcNAcylation coupled to Hippo signaling drives vascular dysfunction in diabetic retinopathy.* Nat Commun, 2024. **15**(1): p. 9334.
40. Zhang, X., et al., *The essential role of YAP O-GlcNAcylation in high-glucose-stimulated liver tumorigenesis*. Nature Communications, 2017. **8**(1): p. 15280.
41. Mo, J.S., et al., *Cellular energy stress induces AMPK-mediated regulation of YAP and the Hippo pathway.* Nat Cell Biol, 2015. **17**(4): p. 500-10.
42. Santo-Domingo, J., et al., *Glucose-dependent phosphorylation signaling pathways and crosstalk to mitochondrial respiration in insulin secreting cells*. Cell Communication and Signaling, 2019. **17**(1): p. 14.
43. Bedford, M.T. and S.G. Clarke, *Protein Arginine Methylation in Mammals: Who, What, and Why.* Molecular Cell, 2009. **33**(1): p. 1-13.
44. Di Lorenzo, A. and M.T. Bedford, *Histone arginine methylation*. FEBS Letters, 2011. **585**(13): p. 2024-2031.
45. Hong, X.-L., et al., *Positive feedback between arginine methylation of YAP and methionine transporter SLC43A2 drives anticancer drug resistance*. Nature Communications, 2025. **16**(1): p. 87.

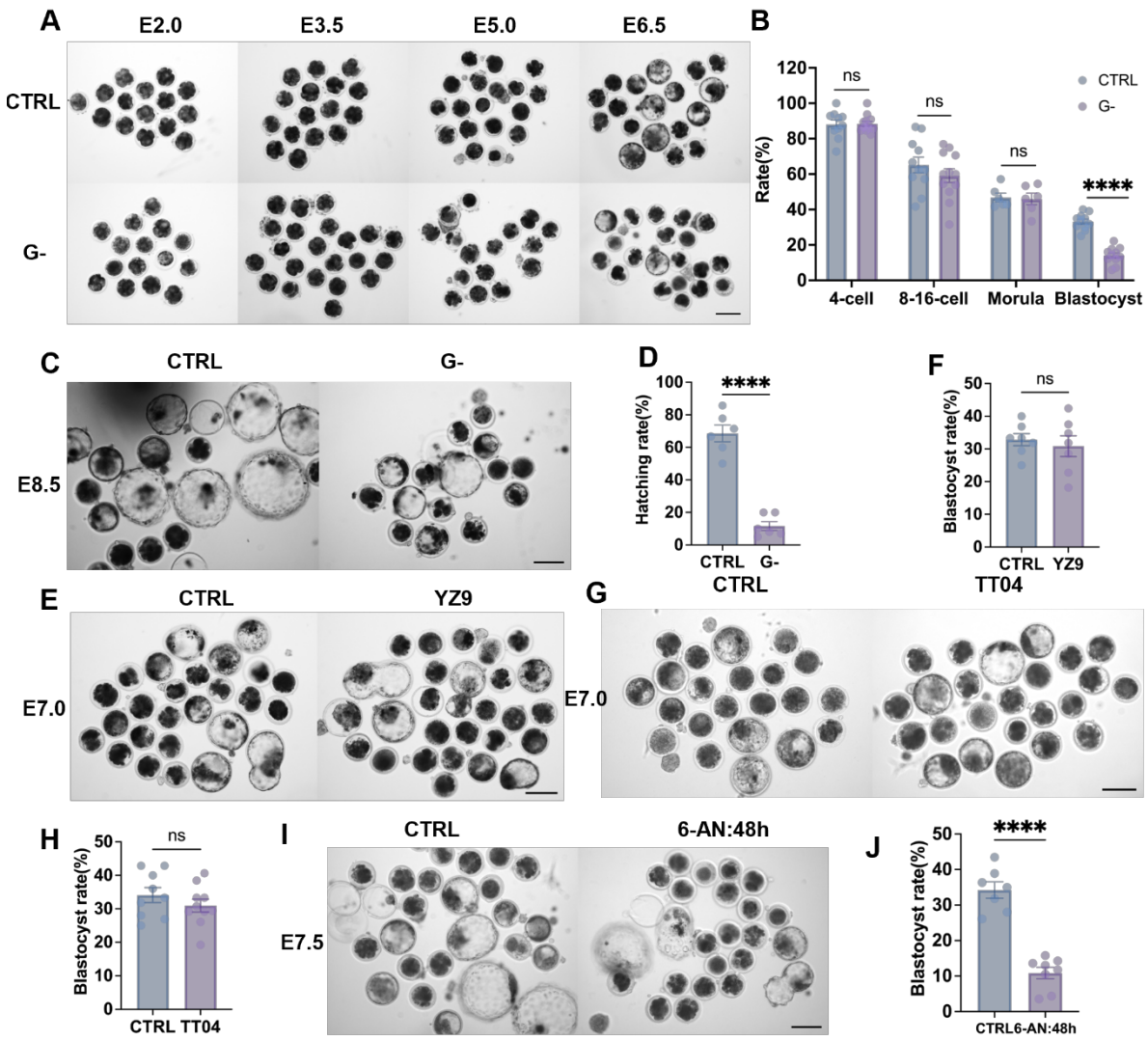

Fig 1 Glucose deprivation and inhibition of glucose metabolism impair bovine embryo development.

(A–D) Representative brightfield images of bovine embryos cultured in G− or CTRL media. Quantification of the proportion of embryos developing to the 4-cell (E2.0), 8–16-cell (E3.5), morula (E5.0), and blastocyst (E6.5) stages, and the proportion of hatching embryos at E8.5.

(E, F) Representative images and corresponding blastocyst formation rates of E7.0 embryos cultured in the presence of the glycolysis inhibitor YZ9, relative to CTRL.

(G, H) Representative images and blastocyst formation rates of E7.0 embryos cultured with the HBP inhibitor TT04, relative to CTRL.

(I, J) Representative images and blastocyst formation rates of E7.5 embryos cultured with the PPP inhibitor 6-AN for 48 hours, relative to CTRL.

All percentages were calculated relative to the total number of zygotes cultured per treatment. Data are presented as mean ± SEM from at least six independent replicates (≥15 embryos per group). Statistical significance was determined using a two-tailed unpaired Student's t-test: ns, not significant; **P < 0.01; ****P < 0.0001. Scale bars, 50 μm.

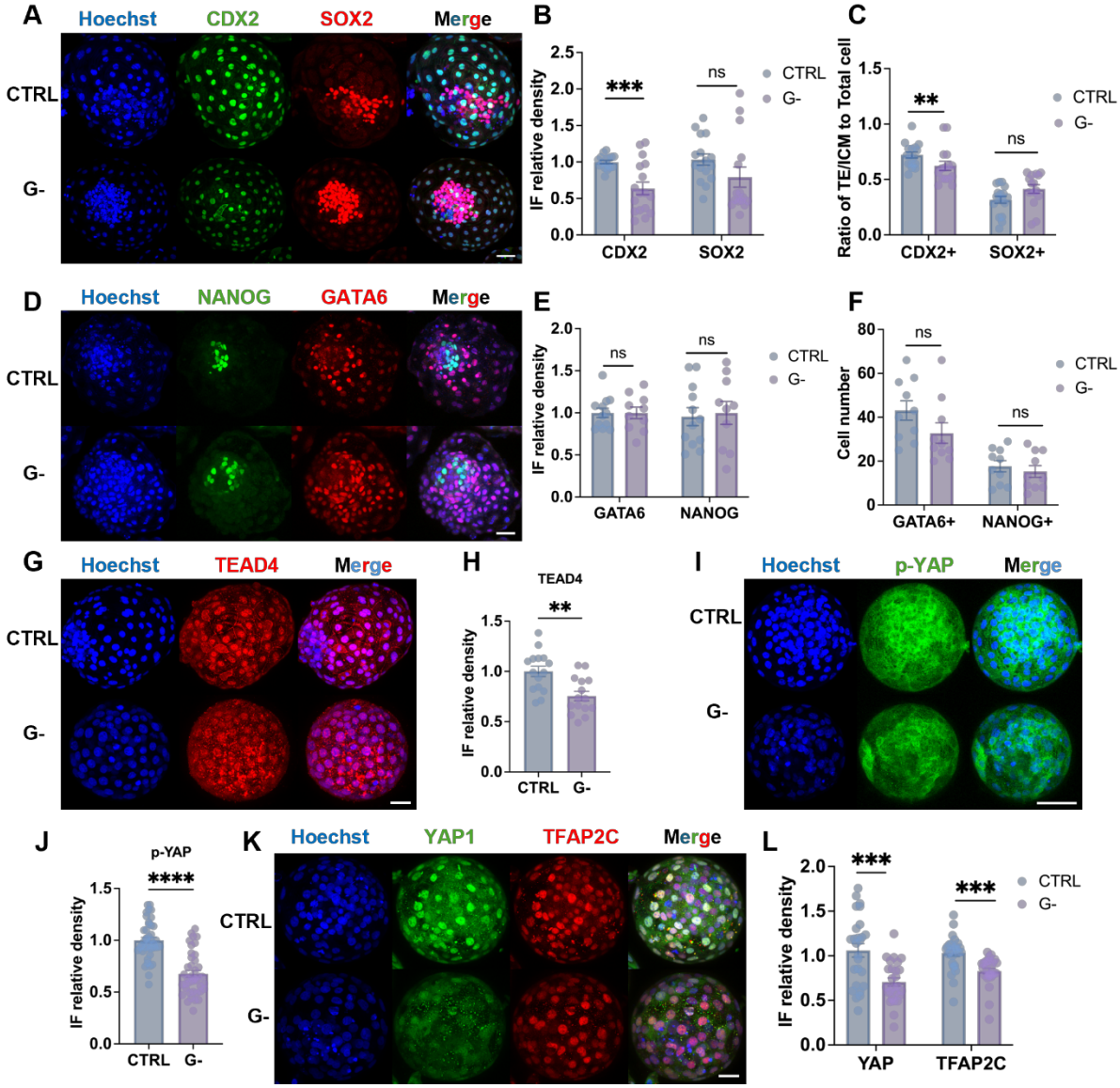

Fig 2 Glucose deprivation suppresses Hippo signaling and impairs TE specification in bovine embryos.

(A–C) Immunofluorescence staining and quantitative analysis of the TE marker CDX2 and ICM marker SOX2 in E7.0 bovine blastocysts cultured under CTRL and G− conditions.

(D–F) Immunofluorescence staining and quantification of EPI marker NANOG and PrE marker GATA6 in E8.5 blastocysts cultured under CTRL and G− conditions.

(G–L) Immunofluorescence staining and quantitative analysis of Hippo pathway components, including TEAD4 (G, H), p-YAP (I, J), YAP (K, L), and TFAP2C (K, L), in E7.0 blastocysts cultured under CTRL and G− conditions.

For quantification, relative lineage-specific cell ratios were calculated for TE ($CDX2^+$/$Hoechst^+$), ICM ($SOX2^+$/$Hoechst^+$), EPI ($NANOG^+$/$Hoechst^+$), and PrE ($GATA6^+$/$Hoechst^+$) populations (n ≥ 3 biological replicates, with ≥3 blastocysts per group). Data are presented as mean ± SEM. Statistical significance was determined using a two-tailed unpaired Student's t-test: ns, not significant; **P < 0.01; ***P < 0.001; ****P < 0.0001. Scale bars, 100 μm.

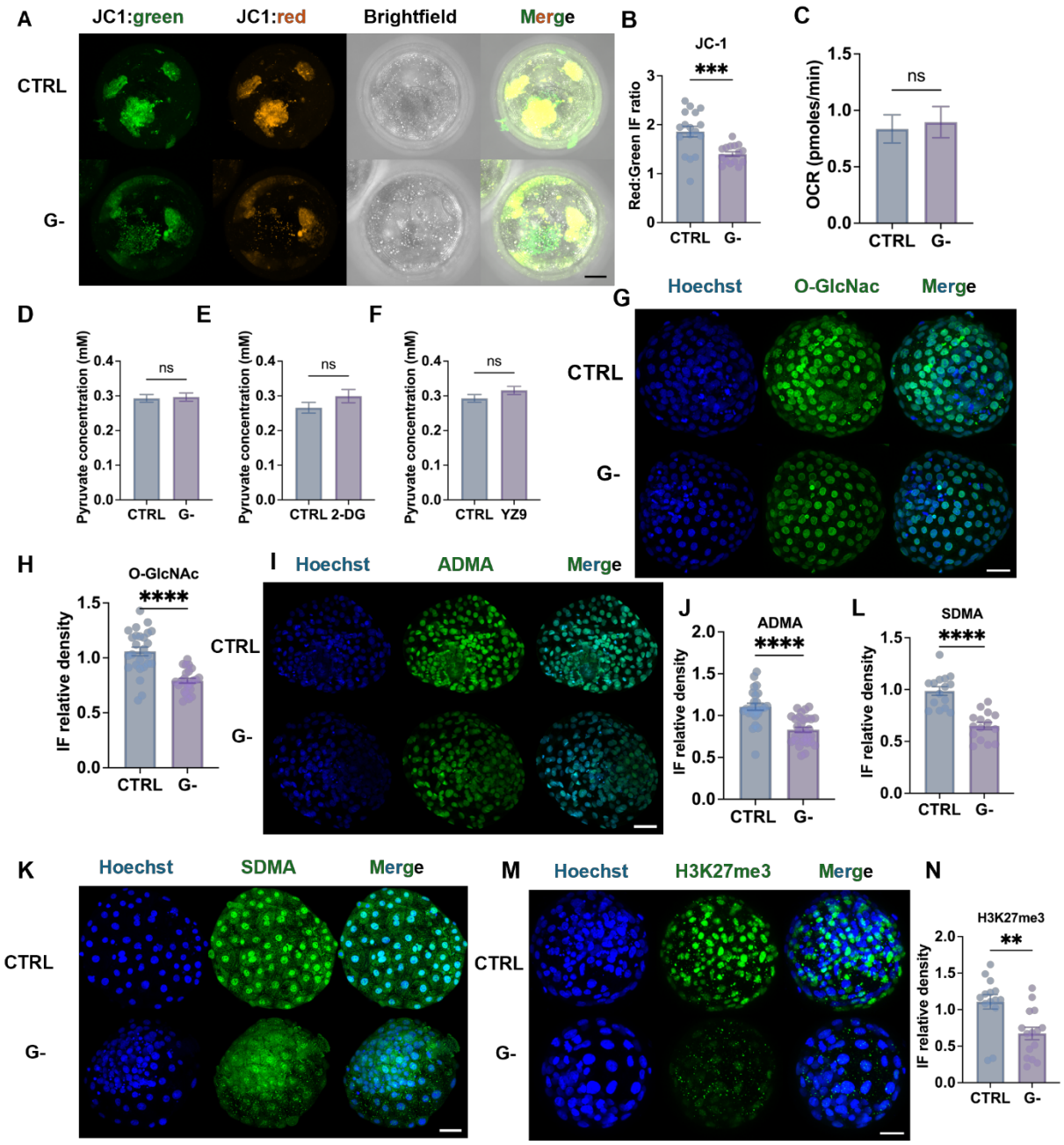

Fig 3 Glucose deprivation disrupts mitochondrial function and biosynthetic metabolism in bovine blastocysts.

(A, B) Representative fluorescence images of JC-1 staining in CTRL and G− blastocysts. Orange fluorescence indicates J-aggregates, whereas green fluorescence indicates J-monomers. Quantification of the red/green JC-1 fluorescence ratio.

(C) OCR measured by Seahorse XF analysis in CTRL and G− blastocysts.

(D–F) Pyruvate concentrations in culture medium following 24 h embryo culture under G−, 2-DG-treated, and YZ9-treated conditions, relative to CTRL.

(G, H) Representative immunofluorescence images and corresponding quantification of global O-GlcNAc (green) levels in CTRL and G− blastocysts.

(I-N) Representative immunofluorescence images and quantification of ADMA, SDMA, H3K27me3 in CTRL and G− blastocysts.

Data are presented as mean ± SEM. Statistical significance was determined using a two-tailed unpaired Student's t-test (n ≥ 3 biological replicates, with ≥5 blastocysts per group): ns, not significant; **P < 0.01; ***P < 0.001; ****P < 0.0001. Scale bars, 100 μm.

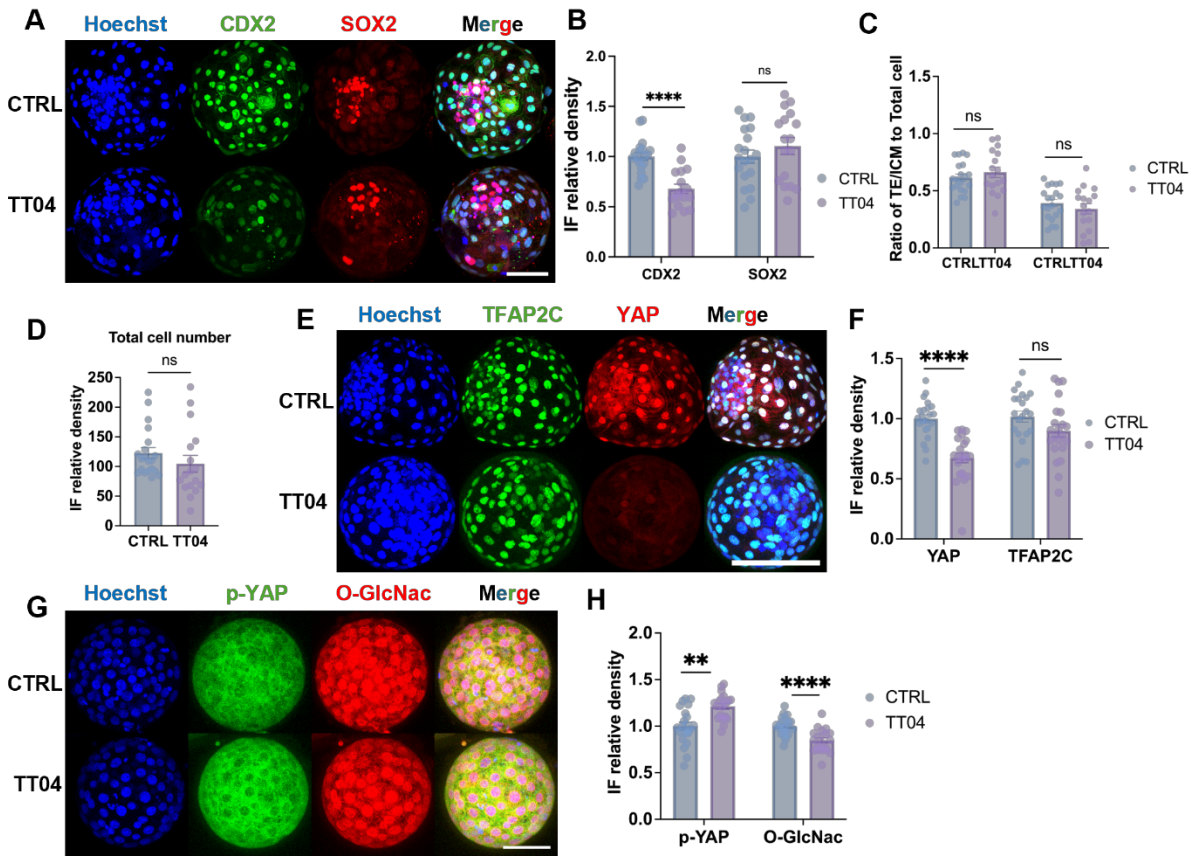

Fig 4 Inhibition of O-GlcNAc disrupts TE specification and Hippo signaling in bovine blastocysts

(A, B) Representative immunofluorescence images and quantitative analysis of CDX2 and SOX2 in E7.0 embryos cultured under CTRL and TT04 treated conditions.

(C, D) Quantitative analysis of total cell number (Hoechst$^+$), and the proportions of TE (CDX2$^+$/Hoechst$^+$) and ICM (SOX2$^+$/Hoechst$^+$) cells in E7.0 embryos cultured under CTRL and TT04-treated conditions.

(E, F) Representative immunofluorescence images and quantitative analysis of YAP and TFAP2C in E7.0 embryos cultured CTRL and TT04 treated conditions.

(G, H) Representative immunofluorescence images and quantitative analysis of p-YAP and global O-GlcNAc in E7.0 embryos cultured CTRL and TT04-treated conditions.

Data are presented as mean ± SEM. n≥3 independent biological replicates, with ≥5 blastocysts per group. Statistical significance was determined using a two-tailed unpaired Student's t-test. ns, not significant; **P < 0.01; ****P < 0.0001. Scale bars, 100 μm.

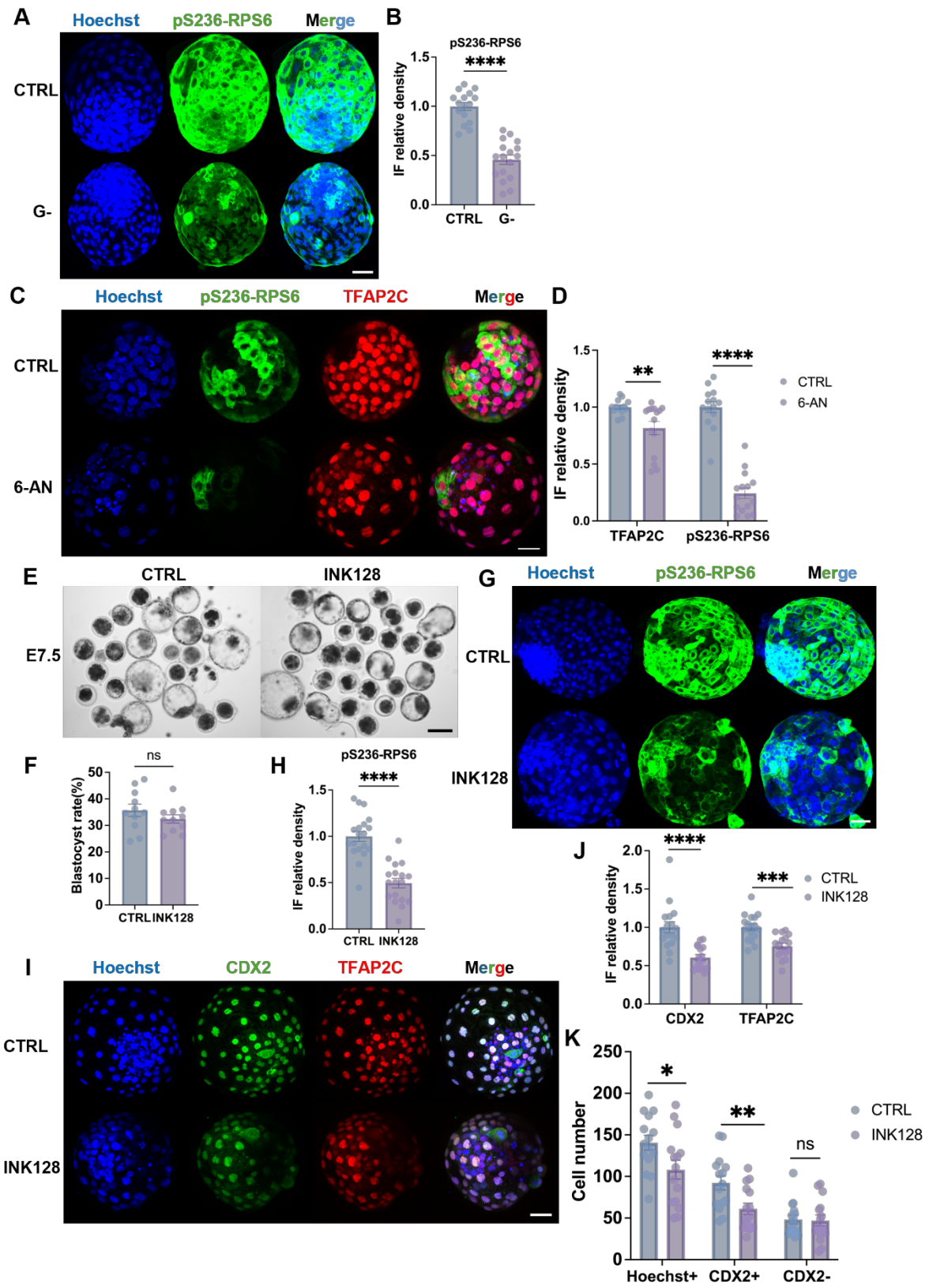

Fig 5 Inhibition of the PPP suppresses mTOR activity and disrupts TE differentiation

(A, B) Representative immunofluorescence images and quantitative analysis of pS236-RPS6 in E7.0 embryos cultured under CTRL or G– conditions.

(C, D) Representative immunofluorescence images and quantitative analysis of pS236-RPS6 and TFAP2C in E7.5 embryos cultured under CTRL or 6-AN-treated conditions.

(E, F) Representative bright-field images and quantification of blastocyst formation rates in E7.0 embryos cultured under CTRL or INK128-treated conditions. Scale bar, 50 μm.

(G, H) Representative immunofluorescence images and quantitative analysis of pS236-RPS6 in E7.5 embryos cultured under CTRL or INK128-treated conditions.

(I–K) Representative immunofluorescence images and quantitative analysis of CDX2 and TFAP2C in embryos under CTRL or INK128-treated conditions.

Data are presented as mean ± SEM. n ≥3 independent biological replicates, with ≥5 embryos per groups. Statistical significance was determined using a two-tailed unpaired Student's t-test: ns, not significant; *P < 0.05; **P < 0.01; ***P < 0.001; ****P < 0.0001. Scale bar, 100 μm

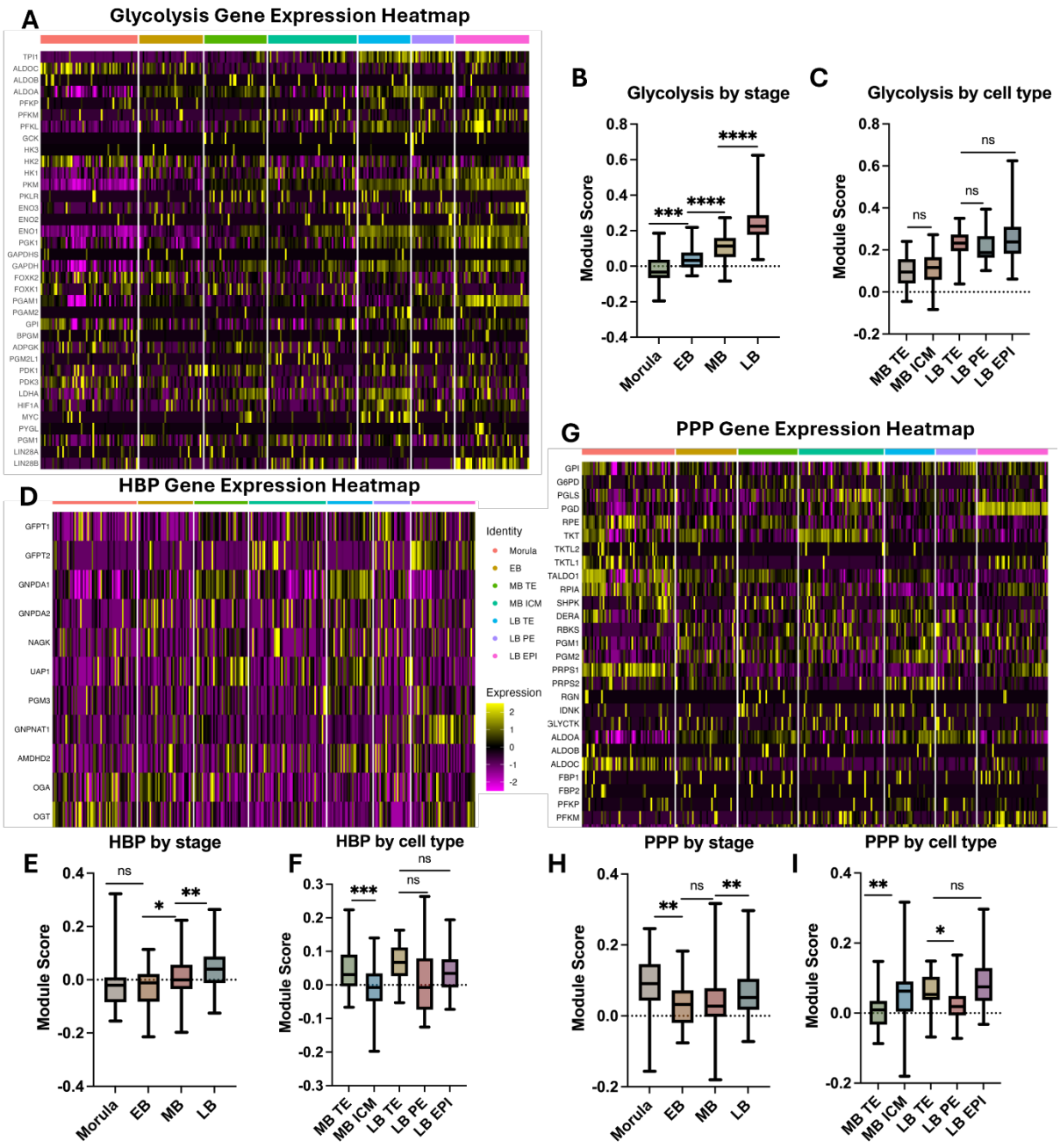

Fig 6 Quantitative analysis of metabolic pathway module scores during bovine preimplantation development.

(A, D, G) Heatmap showing the expression of glycolysis,HBP and PPP module genes.

(B, E, H) Bar graphs comparing the dynamic changes in module scores of glycolysis, HBP and PPP across grouped developmental stages.

(C, F, I) Bar graphs illustrating the differences in module scores among TE, ICM, PE and EPI at the mid- and late-blastocyst stages.

Data are presented as mean ± SEM. Statistical significance was determined using a two-tailed unpaired Student's t-test: ns, not significant; *$P < 0.05$; **$P < 0.01$; ***$P < 0.001$; ****$P < 0.0001$.